MULTIMODAL MEDICAL VOLUME REGISTRATION BASED ON SPHERICAL MARKERS

M. Čapek, R. Wegenkittl*, A. Koenig, W. Jaschke***, R. Sweeney****, R. Bale***

VRVis – Research Center for Virtual Reality und Visualization
Lothringerstrasse 16/4, 1030 Vienna, Austria, e-mail: capek@vrvis.at
*TIANI Medgraph GmbH, Campus 21, Liebermannstrasse A01303,
2345 Brunn am Gebirge, Austria, e-mail: rainer@tiani.com
**Institute of Computer Graphics, Vienna University of Technology,
Favoritenstrasse 9/5 Stock, 1040 Vienna, Austria, e-mail: koenig@cg.tuwien.ac.at
***Interdisciplinary Stereotactic Interventional Planning Laboratory (SIP Lab), University Department of
Radiology I, Anichstrasse 35, 6020 Innsbruck, Austria, e-mail: reto.bale@uibk.ac.at, werner.jaschke@uibk.ac.at
**** University Department of Radiotherapy-Oncology, Anichstrasse 35, 6020 Innsbruck, Austria
e-mail: reinhart.sweeney@uibk.ac.at

ABSTRACT

We propose volume registration procedures based on spherical artificial markers presented in medical multimodal data sets (MRI and CT, especially). The procedures proposed are either semi-automatic or fully-automatic. A semi-automatic approach requires to label approximate locations of the spherical markers in the data sets and then registration operates autonomically. A fully-automatic approach does not require any user interaction, i.e. all registration subtasks – namely segmentation of spheres, finding the correspondence between two sets of spheres and, finally, computing geometrical transformation that maps the first set of spheres onto the second one – are performed automatically by the computer.

Keywords: multimodal medical registration, markers, segmentation, iterative closest point algorithm.

1. INTRODUCTION

Nowadays, volume registration becomes a task required by more and more physicians and researchers in the area of medical volume processing and visualization. In this context the term "volume registration" is used for the rectification of mutual position of objects presented in several volume data sets in order to obtain their integrated display giving a comparison and more comprehensive information.

The integrated display is used for medical diagnosis, surgery planning, and comparison of pre-operative and post-operative human brains, etc. It is assisted by different tomographic imaging modalities like computed tomography (CT) and magnetic resonance imaging (MRI), because these modalities provide supplementary information (CT – bones vs. MRI – brain matter) and their integration improves the spatial understanding of anatomical structures.

A variety of approaches to the volume registration problem have been published until now.

Good surveys are given by [Brown92] and [Maint98]. These approaches can be split into two main groups: methods based on features [Maure96] or markers [Ranga97] extracted from volume data sets and methods using voxel information directly without any pre-segmentation.

Voxel-based methods [Woods93], [Maes97] are most popular today, since they are fully automatic and robust. However, these methods have greater registration error in general, especially in case of multimodal data sets. Additionally, these methods are more computationally demanding when compared with methods based on artificial markers. Voxel-based registration methods have been reported among others in [Čapek99], [Čapek00].

For the planning of brain surgery a precise and fast registration of multimodal volumes is needed. This can be achieved especially by a method based on artificial markers [Tiche94]. Therefore, an external reference frame "SIP Lab Innsbruck frame" [Bale97a, 97b, 00] containing twelve sphere-shaped

markers has been created (see Figure 1). The position of the markers is unambiguous, therefore, only one correct match of all the markers from two different data sets exists. The frame is fixated on the patient's head in an exact position by means of "Vogele-Bale-Hohner (VBH) mouthpiece" [Marti98] during his investigation by the tomographic modalities (see Figure 2). The mouthpiece guarantees the identical relationship of the markers to the cranial anatomy and, thus, accurate registration.

Among the main advantages of the described method are the facts that it is non-invasive (markers are not implanted into the patient's skull), fully automatic, precise, fast and reproducible.
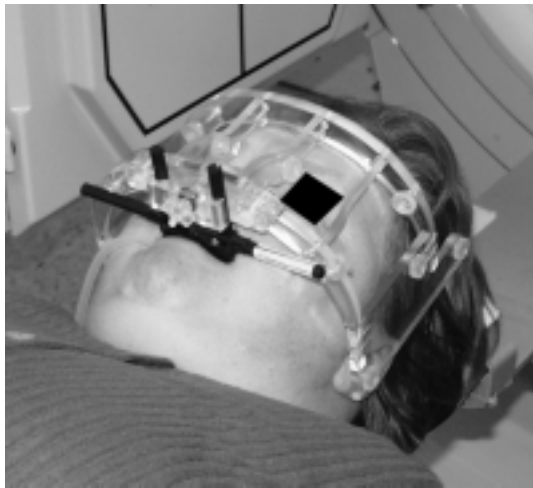

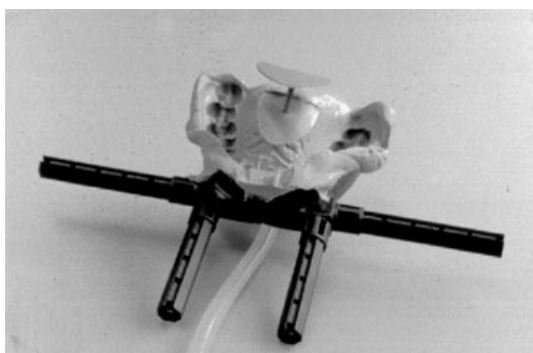Figure 1: "SIP Lab Innsbruck frame" fixated on the patient's head

Figure 2: "Vogele-Bale-Hohner (VBH) mouthpiece" that is fixated against the patient's upper plate in his mouth by means of vacuum

2. DATA

Data sets of two modalities are to be registered: CT and MRI. Resolution of CT volumes is 512 x 512

pixels per slice and up to 200 slices. Resolution of MRI is lower – 256 x 256 pixels per slice and about 200 slices.

Figure 3 depicts a CT rendered image of a patient's head wearing the "SIP Lab Innsbruck frame". In case of CT this frame is well visible and, thus, makes segmentation of markers more difficult when compared with MRI that is without the frame (see Figure 5). Figure 4 shows a slice of a CT volume with two markers – white circles on the left and right side of the image.

Due to the material used the "SIP Lab Innsbruck frame" itself is not visible in MRI volume (Figure 5), only separate markers can be seen. The patient's mouth is open, since the frame is fixated on the head by the "Vogele-Bale-Hohner (VBH) mouthpiece" against the patient's upper plate in his mouth by means of vacuum (Figure 2). Figure 6 presents a MRI slice with one marker on the left side. Note that MRI slices are sagittal while CT slices are axial.

3. METHODS

The overall work-flow of this marker-based registration consists of four steps: segmentation of markers in both data sets and finding their centers of gravity, finding correspondence among the centers, least squares evaluation of geometrical transformation and, finally, visualization of the result of registration.

Both semi-automatic and fully-automatic approaches are described in this paper. The methods applied to solve individual registration steps differ somewhat.

SEMI-AUTOMATIC APPROACH

Before registration can be started, the approximate locations of all spheres in both data sets have to be labeled by the user. The order of labeling is not important. It is also not necessary to label the spheres exactly, since an automatic search for a sphere in the close neighborhood of the label is performed next.

In general the sphere markers are the brightest objects in the data sets, but due to possible artifacts the overall brightness of some spheres can be lower. Therefore, a threshold-independent technique has to be used for their segmentation. We propose the following.
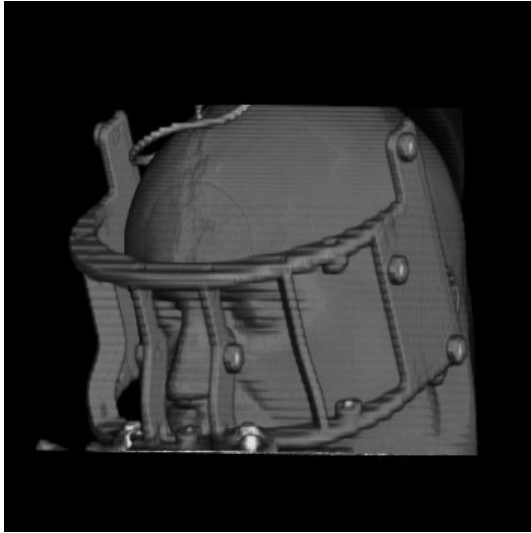
Figure 3: 3D rendered CT image of a head with the "SIP Lab Innsbruck frame" containing the spherical markers
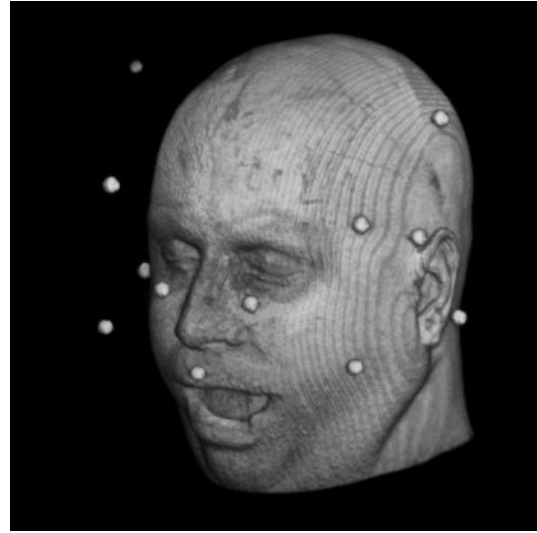

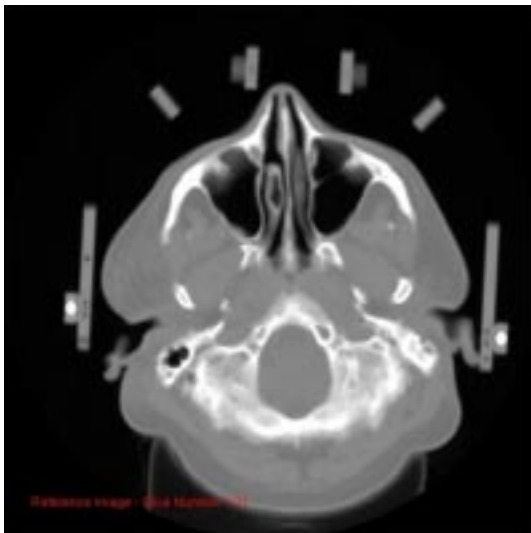
Figure 5: 3D rendered MRI image of a head

Figure 4: CT slice with two markers (the white circles)

Figure 6: MRI slice with one marker
(a white circle is on the left)

When the label point is specified by the user, the maximum gray value is found in its pre-defined 3D neighborhood. A histogram of gray values of this neighborhood is generated. Since the volume of the spheres in mm^3 is known and the spheres contain the brightest gray values, it is assumed that the brightest voxels of the histogram belong to the sphere (see Figure 7). Segmentation of the sphere is accomplished by 3D region growing [Žára98]. It uses the brightest voxel of the histogram as a seed and the darkest value belonging to the sphere as a threshold which is determined automatically. During segmentation, the centers of gravity of spheres are computed simultaneously. This histogram-driven region growing technique is applied successfully for segmentation of markers in both CT volumes and MRI volumes.

Using this method two sets of points that correspond to the centers of gravity of the spheres have been generated. Since all the spheres (and their centers of gravity) in both data sets are found without any false or missing ones, it is possible to apply the ICP (iterative closest point) algorithm [Besl92] to find their correspondence as well as computing a least square estimation of geometrical transformation.
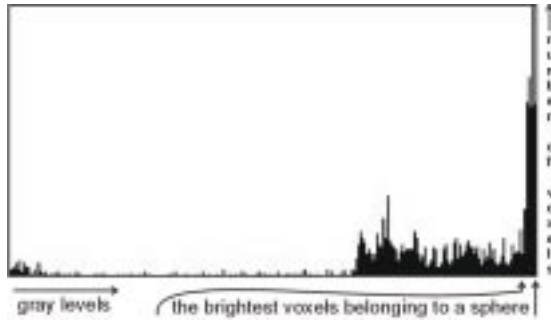
Figure 7: Histogram-driven sphere segmentation

ICP starts by pairing points (centers of gravity of the spheres) from both sets according to the minimum of their Euclidian distances. Then the parameters of the geometrical transformation[1] are computed by using SVD (singular value decomposition) [Press92]. The obtained parameters are applied to one set of points. These two steps are iteratively repeated until a local optimum is achieved.

Since ICP converges to a local optimum only, we use a stochastic approach to obtain a global optimum. Our stochastic approach hinges on repeated random selection of an initial geometrical transformation which enters the ICP algorithm.

After finding the global optimum, which is indicated by a value of a mean squared error of the registration approaching zero, one volume data set is recomputed with respect to the second one and displayed.

FULLY-AUTOMATIC APPROACH

First of all, an automatic segmentation of spheres is performed. This segmentation consists of two steps: first, a global threshold is applied to the whole data set in order to transform it into a binary representation. 3D region growing is applied to it. Individual objects are evaluated by means of simple characteristics like the similarity to a sphere. The characteristics are the size (volume) of an object and its maximal diameter.

The exact segmentation of the sphere markers together with computation of their centers of gravity follows by using the histogram-driven 3D region growing described in the previous section.

This two-step segmentation technique is simple and fast even for 3D data sets. However, its

reliability depends on the determination of the global threshold in the first step. Therefore, it may happen that, although most of the spheres are segmented successfully, some spheres can be missing or incorrectly segmented. The ICP algorithm is sensitive to missing points and cannot be applied in this case. Hence, a procedure that pairs corresponding points must be employed before.

An "elegant" procedure for this purpose has been described in [Skea93]. However, it is intended for the 2D case only and, thus, it had to be extended to 3D. Using the main idea of this procedure and changing a criterion used by it yields the desired algorithm.

This procedure ("accumulator algorithm") is based on pairing similar triangles made from points in two point sets. Every possible triangle created from points in the first point set is compared with all possible triangles made from points in the second point set. If two triangles are similar according to a criterion (mentioned below) then an accumulator is updated. The accumulator is rectangular and has the size M x N where M and N represent the number of points in the two point sets. For similar triangles cells of the accumulator belonging to corresponding vertices of both triangles are incremented by 1. After testing all pairs of triangles, cells that correspond to properly paired points contain the highest values while cells of spurious points have the lowest values.

The original criterion for measuring the similarity of triangles [Skea93] is suitable only for the 2D case and, therefore, it had to replaced by a criterion applicable to 3D. We decided to apply a criterion based on aspect ratios of side lengths of triangles: two triangles are similar if aspect ratios $\left(a/\bar{a}, b/\bar{b}, c/\bar{c}\right)$ of all their sides differ only by a predefined tolerance ε (see Figure 8).
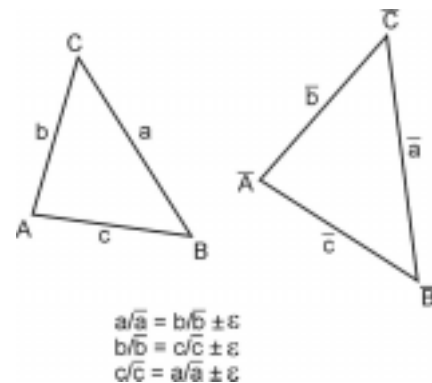

$$a/\bar{a} = b/\bar{b} \pm \varepsilon$$
$$b/\bar{b} = c/\bar{c} \pm \varepsilon$$
$$c/\bar{c} = a/\bar{a} \pm \varepsilon$$

Figure 8: Aspect ratios of the sides of two triangles

---

[1] Rigid-body transformation, i.e. translation, rotation and scaling in 3D space.

Since all possible triangles have to be tested, the algorithm is time-consuming for large point sets. Fortunately, the datasets produced by the described method consists of twelve points per data set typically, which keeps the calculation short (typically tens of miliseconds).

After finding a correspondence between the two point sets by the accumulator algorithm, the ICP algorithm can be applied to find the resulting geometrical transformation. Once it has been found, one volume data set is recomputed with respect to the second one and displayed.

4. RESULTS

The described registration methods were applied to multimodal data sets of a human head. The methods were compared with the manual approach in terms of accuracy and speed.

The accuracy of the registration is expressed by the mean squared error

$$e^2(R,t,c) = \frac{1}{n}\sum_{i=1}^{n}\left\| y_i - (cRx_i + t) \right\|^2 \qquad (1)$$

where R stands for rotation, t for translation, c for scaling, n for the number of points and x_i and y_i for the two sets of points. The speed T expresses the time necessary either for labeling the markers by an experienced user (manual or semi-automatic approach) or for automatic segmentation of the markers (fully-automatic approach). These timings illustrate how semi- and fully-automatic methods accelerate work in real practice.

Method	e^2	T [sec]
Manual	2.1159	300-400
Semi-automatic	0.3736	150-200
Fully-automatic	0.3736	15-120[*]

Table 1: Comparison of different point matching methods

First, the same pair of data sets was registered manually by one user five times, second, semi-automatically again five times and, finally, once fully-automatically. The results of average values are collected in Table 1.

Although the manual method takes longest time, it gives the highest registration error. This is not surprising, since during registration the user has to specify centers of gravity of the spheres manually. This specification is time-consuming and yet not exact. The accuracy of the semi- and full-automatic methods is the same, because the same method for finding the centers of gravity of the spheres is used, but the fully-automatic approach is faster than the semi-automatic one.

In case of the fully-automatic approach the combination of accumulator algorithm and ICP algorithm proved to be an efficient and robust point matching strategy. It was mentioned above that the successful detection of the sphere markers depends on the determination of the global threshold used in the two-step segmentation. However, the applied combination enables us to achieve successful registration even if the global threshold varies to an extent of approximately 20% of a maximal gray level in CT data sets and to an extent of approximately 40% of a maximal gray level in MRI data sets (the mentioned percentages were determined experimentally). On the borders of these extents fewer (e.g. 10) or more (e.g. 14) markers used to be found than it were expected (12), but the proposed combination finds correct markers and still performs successful registration. If stand-alone ICP algorithm is applied, registration is not always successful. Table 2 shows how the number of markers – including false ones eventually – found by the two-stepped segmentation, the number of proper pairs of markers, and accuracy of registration vary if different global thresholds are applied to one pair of multimodal data sets. The last column of the table indicates some events when the stand-alone (s.-a.) ICP algorithm fails, i.e. it gives higher registration errors than the combinations of both the algorithms.

CT global threshold/ number of found markers	MRI global threshold/ number of found markers	number of proper marker pairs	e^2 (accum. alg. + ICP alg.)	e^2 (ICP alg. s.-a.)
1400/12	*50/12*	*12*	*0.3736*	*0.3736*
1200/10	50/12	9	0.4354	52.685
1300/13	100/12	11	0.3285	731.006
1400/12	150/15	11	0.3285	1218.499
1500/13	200/11	11	0.3285	0.3285
2000/13	220/10	9	0.3422	865.86

Table 2: Fully-automatic registration results for different global thresholds applied (see text for explanation).

---

[*] Depends on the sizes of input data sets and computational power of a used computer (the timings are for a Pentium III/600 MHz/512 MB).
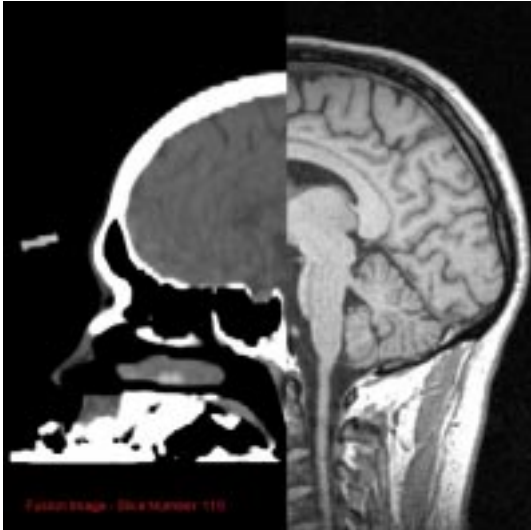
Figure 9: 2D example of a sagittal CT-MRI fusion image before (the upper image) and after registration (the lower image); (CT - the left part /windowed for highlighting inner structures of the brain/, MRI - the right part)
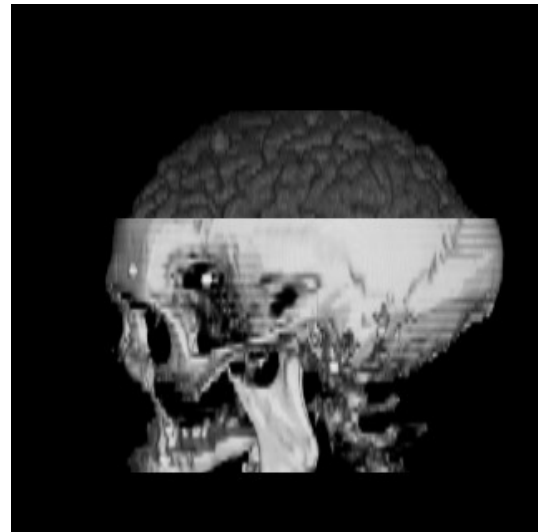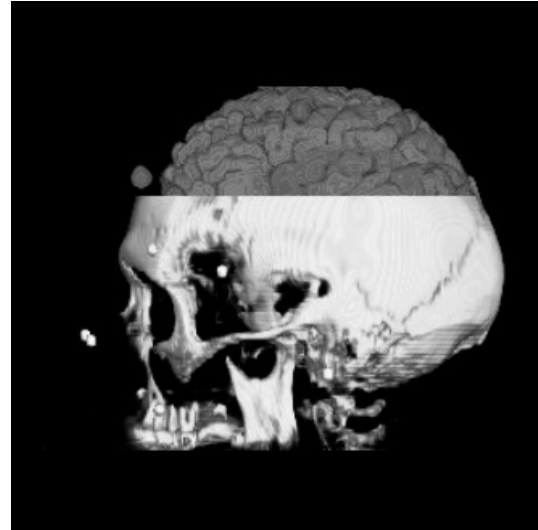

Figure 10: 3D example of a CT-MR fusion image with sphere markers before (the upper image – the brain touches and exceeds the skull) and after registration (the lower image); (CT - the bottom part /bones segmented/, MRI – the upper part /the brain segmented/)

In the first line (*in cursive*) there are values of the optimal thresholds of the tested pair of data sets. Other lines correspond to increasing values of thresholds approximately in the ranges that are mentioned above. From Table 2 (the fourth column) follows that acceptable accuracy of registration is preserved for wide ranges of thresholds applied to input data sets. Lower values of registration error e^2 for the higher thresholds are caused by the lower number of marker pairs and, thus, by the lower number of error contributions (see Formula (1)). The stand-alone ICP algorithm fails in the cases when false markers are found in both the data sets (i.e. not only in one data set – see the 2-nd, 3-rd, 4-th and 6-th row in the fifth column of Table 2).

Figures 9 and 10 exemplify fusion images of registration results (obtained by the fully-automatic approach). For both figures the reference volume was MRI. Every time the second data set (floating) was re-mapped according to the found geometrical transformation, see Figure 11. Figure 9 depicts a 2D example of CT-MRI registration where the CT volume was windowed in order to highlight inner structures of the brain. One can see that theses structures are well registered (the lower image). Figure 10 shows a 3D image of CT-MRI registration

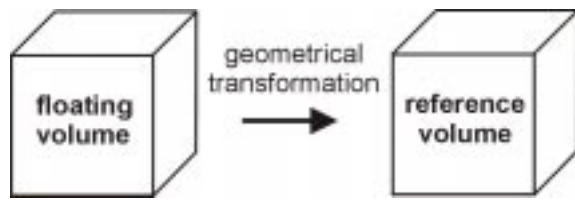where bones were segmented in the CT volume and the brain in the MRI volume.

Figure 11: Re-mapping a floating volume according to a reference one

5. CONCLUSION

A semi-automatic and a fully-automatic method for multimodal registration based on artificial spherical markers are presented. These approaches were chosen, because the medical practice requires fast, precise and reliable methods that are affected neither by the difference in modalities used, nor by the change of illumination, contrast etc. The methods used have proven to be suitable for medical purposes and will be applied for head surgery planning, jaw surgery and external head radiation treatment [Swealen98].

The electronic version of this article can be obtained via http://www.tiani.com/research.

6. ACKNOWLEDGEMENTS

REFERENCES

[Bale97a] Bale, R.J., Vogele, M., Martin, A., Auer, T., Hensler, E., Eichberger, P., Freysinger, W., Sweeney, R., Gunkel, A.R., Lukas, P.H.: VBH head holder to improve frameless stereotactic brachytherapy of cranial tumors. Comput Aided Surg 1997;2(5):286-91.

[Bale97b] Bale, R.J., Vogele M., Freysinger W., Gunkel A.R., Martin A., Bumm K., Thumfart W.F.: Minimally invasive head holder to improve the performance of frameless stereotactic surgery. Laryngoscope 1997 Mar;107(3):373-7.

[Bale00] Bale R., Burtscher J., Eisner W., Obwegeser A., Rieger M., Sweeney R.A., Dessl A., Giacomuzzi S.M., Jaschke W.: Computer assisted neurosurgery with a non-invasive vacuum-dental cast acting as reference base – another step towards a unified approach in the treatment of brain tumors. J Neurosurg 2000 Aug;93:208-213.

[Besl92] Besl, P. J., McKay, N. D.: A Method for Registration of 3-D Shapes, IEEE PAMI, Vol. 14, No. 2, February 1992, pp. 239-256.

[Brown92] Brown, L. G.: A Survey of Image Registration Techniques. ACM Computing Surveys, Vol. 24, No. 4, p. 325-376, December 1992.

[Čapek99] Čapek, M.: Optimization Strategies Applied to Global Similarity Based Image Registration Methods. In: WSCG'99 Conference proceedings. Vol. 1., Pilsen: University of West Bohemia. 1999, pp. 369-374.

[Čapek00] Čapek, M., Trojanová, H.: Two-Stage Multimodality Medical Volume Registration. In: WSCG´2000 Conference proceedings. Vol. 1., Pilsen: University of West Bohemia, 2000, pp. 155-160.

[Maes97] Maes, F., Collignon, A., Vandermeulen, D., Marchal, G., Suetens, P.: Multimodality Image Registration by Maximization of Mutual Information. IEEE Trans. Med. Imag., Vol. 16, No. 2, p. 187-198, April 1997.

[Maint98] Maintz, J. B. A., Viergever, M. A.: A Survey of Medical Image Registration, Medical Image Analysis, Vol. 2, No. 1, pp. 1-36, 1998.

[Marti98] Martin A., Bale R.J., Vogele M., Gunkel A.R., Thumfart W.F., Freysinger W.: Vogele-Bale-Hohner mouthpiece: registration device for frameless stereotactic surgery. Radiology 1998 Jul; 208 (1): 261-5.

[Maure96] Maurer, C. R., et al.: Registration of 3-D Images Using Weighted Geometrical Features. IEEE Trans. Med. Imag., Vol. 15, No. 6, p. 836-849, December 1996.

[Press92] Press, W. H., et al.: Numerical Recipes in C, The Art of Scientific Computing. 2nd ed., Cambridge University Press, 1992, 994 pages.

[Ranga97] Rangarajan, A., et al.: A Robust Point-Matching Algorithm for Autoradiograph Alignment. Medical Image Analysis, Vol. 1, No. 4, p. 379-398, 1996/7.

[Skea93] Skea, D., et al.: A Control Point Matching Algorithm. Pattern Recognition, Vol. 26, No. 2, 1993, pp. 269-276.

[Sween98] Sweeney R., Bale R., Vogele M., Nevinny-Stickel M., Bluhm A., Auer T.,

Hessenberger G., Lukas P.: Repositioning accuracy: comparison of a non-invasive head holder with thermoplastic mask for fractionated radiotherapy and a case report. Int J Radiat Oncol Biol Phys 1998 May 1;41(2):475-83.

[Tiche94] Tichem, M., Cohen, M. S.: Subμm Registration of Fiducial Marks Using Machine Vision. IEEE Trans. Pattern Anal. Machine Intell., Vol. PAMI-16, No. 8, p. 791-794, August 1994.

[Woods93] Woods, R. P., Mazziotta, J. C., Cherry, S. R.: MRI-PET Registration with Automated Algorithm. *Journal of Computer Assisted Tomography*, Vol. 17, No. 4, p. 536-546, July/August 1993.

[Žára98] Žára, J., Beneš, B., Felkel, P.: Modern Computer Graphics. Computer Press, Prague, 1998, 448 pages. (in Czech)